PHYSICAL REVIEW D VOLUME 18, NUMBER 9 1 NOVEMBER 1978

K^+p scattering analysis to 2 GeV/c

Richard A. Arndt and L. David Roper
Virginia Polytechnic Institute and State University, Blacksburg, Virginia 24061

Phillip H. Steinberg
University of Maryland, College Park, Maryland 20742

(Received 21 February 1978)

The K^+p scattering data up to 2 GeV/c were fitted with a coupled-channel K-matrix parametrization in which inelasticity is represented by a single production channel for each partial wave. Several solutions are possible above laboratory kinetic energies about 1 GeV, but all are essentially the same below this energy. All solutions that we have found have a P_{13} resonance pole at about total c.m. energy $(1796-i101)$ MeV. Resonance poles are present in other partial waves but are at considerably higher energies or are considerably farther from the real energy axis. More reliable measurements of polarizations are needed to firmly establish the existence of resonance poles other than the P_{13} one. Also, contemporary measurements of the reaction cross sections are needed.

I. INTRODUCTION

This is a more complete account of work reported by the authors in a 1974 Letter.[1] That earlier brief report has been criticized[2] for not agreeing with recently measured polarization values[3] at low energies. In the more complete work reported herein, the low-energy P waves are increased such that the new polarization values are well fitted. Contrary to the criticism,[2] the P_{13} pole previously reported at $(1787-i100)$ MeV remains, but is shifted slightly to $(1796-i101)$ MeV. (Notation: Partial waves are denoted by $l_{T,2J}$, where l is the orbital angular momentum of the scattering state in spectroscopic notation, T is the isotopic spin, and J is the total angular momentum.)

An analysis by B. R. Martin[4,2] also reports a P_{13} pole at $(1820-i134)$ MeV. This analysis did not use the recent polarization data[3,6] that are used in the analysis reported here. We fitted our amplitude parametrization (see below) to Martin's partial waves, but could not achieve a good fit to our data set (described below) by subsequently varying the parameters. Therefore, we conclude that the solutions reported below are better representations of the data than is Martin's solution, because our solutions do fit the data reasonably well.

Another analysis by Cutkosky *et al.*[7] is not in a form to facilitate locating pole positions; however, they state that "no significant improvements were found in the fit to the dispersion relations when explicit resonance poles were inserted in the S and P waves." Of course, that would not exclude the possibility of a pole in the P_{13} state. In fact, we found a P_{13} pole at $(1934-i101)$ MeV when we fitted our parametrization to their partial waves; but we could not achieve a good fit to our data set by subsequently varying the parameters. (This solution was originally obtained without the benefit of the Abe *et al.*[5] precise differential-cross-section data or the recent polarization data.[3,6] Therefore, we conclude that this solution is not as good a representation of the data as are the solutions reported below.

We have revised our previously reported[1] solution in order to fit the recent low-energy polarization measurements, and have found several possible behaviors at the highest energies. In this paper we report two of the solutions and indicate the kinds of measurements that need to be made in order to distinguish among the possible solutions.

In the next section we present our criteria for data selection; the list of data used is in the Appendix. Section III contains an outline of the parametrization we used in our fits and Sec. IV describes the solutions we obtained. In Sec. V we show how well the solutions fit the data. A description of the most important characteristics of our solutions is given in Sec. VI, and Sec. VII delineates experiments that need to be done in order to better determine the partial-wave amplitudes for K^+p scattering.

II. DATA

The data references used in our fit are given in the Appendix. Seven new references that were not included in the 1975 CERN K^+p bibliography[8] are starred. These new data are (1) calculated values at 0.1 GeV/c and 0.15 GeV/c intervals of $\alpha = \mathrm{Re}f(0)/\mathrm{Im}f(0)$, where $f(\theta)$ is the non-spin-flip scattering amplitude, reported in data references 76B1 and 76B2, (2) very precise and copius differ-

ential cross sections, beginning at laboratory kinetic energies 502 MeV, reported in data reference 75A1 (these data were reported in preliminary form in the CERN bibliography reference 73A2), (3) polarization and differential cross sections at 1277 MeV reported in data reference 75P1, (4) polarizations at four energies from 322 to 567 MeV reported in data reference 76E1, (5) a reaction cross-section value at 1373 MeV reported in data reference 77M1, and (6) low-energy differential cross sections from 66.5 to 274 MeV and a reaction cross section at 274 MeV in data reference 74B1. All of these new data are included in our data set.

Some of the older differential cross-section data are redundant with the data of data reference 75A1 and are rendered useless to the fit by the high precision and copious values of the new data of 75A1. We have eliminated all such data from our set. Also, many of the older data are in great disagreement with the 75A1 data and do nothing but cause a large contribution to χ^2 (goodness-of-fit parameter) because of the extremely small errors on the 75A1 data. We have eliminated these data.

There is great disagreement among the total cross-section data. Prior to fitting we eliminated some of these data that are obviously in disagreement with the large body of the data. In the course of fitting we eliminated some more of these data whose disagreement with the large body of the data was made more obvious by the fit.

We kept all reaction cross sections in our data

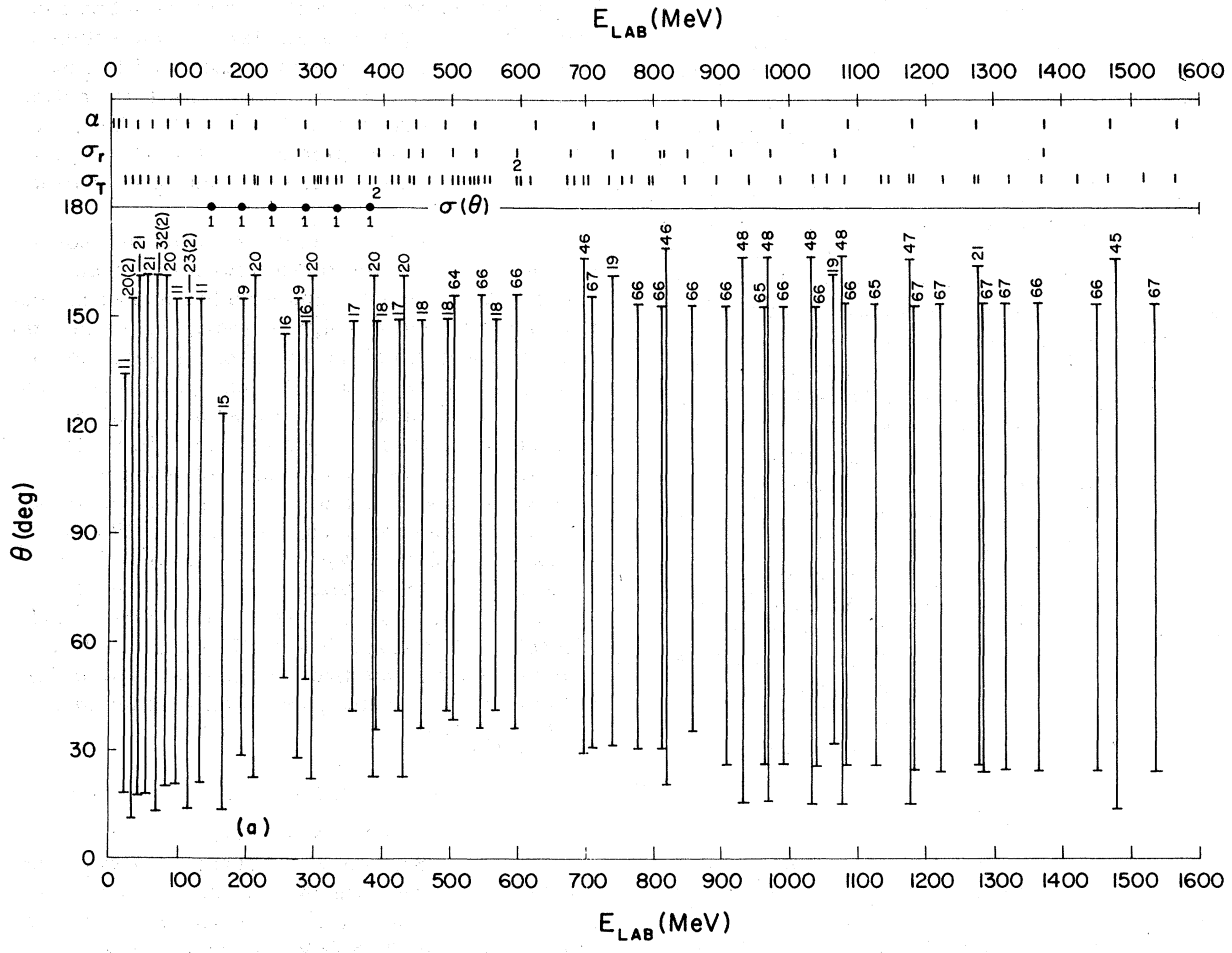

FIG. 1. (a) Laboratory-kinetic-energy locations of $\alpha = \mathrm{Re}f(0)/\mathrm{Im}f(0)$, σ_r, σ_T; and $\sigma(\theta)$ data used in our analysis. Also indicated are the angular range and number of angles for the $\sigma(\theta)$ data. Number of experiments at an energy are in parentheses for $\sigma(\theta)$. Number by σ_T or σ_r entries indicates number of experiments. (b) Laboratory-kinetic-energy locations of $P(\theta)$ used in our analysis. Also indicated are angular range and number of angles. Number of experiments at an energy are in parentheses.

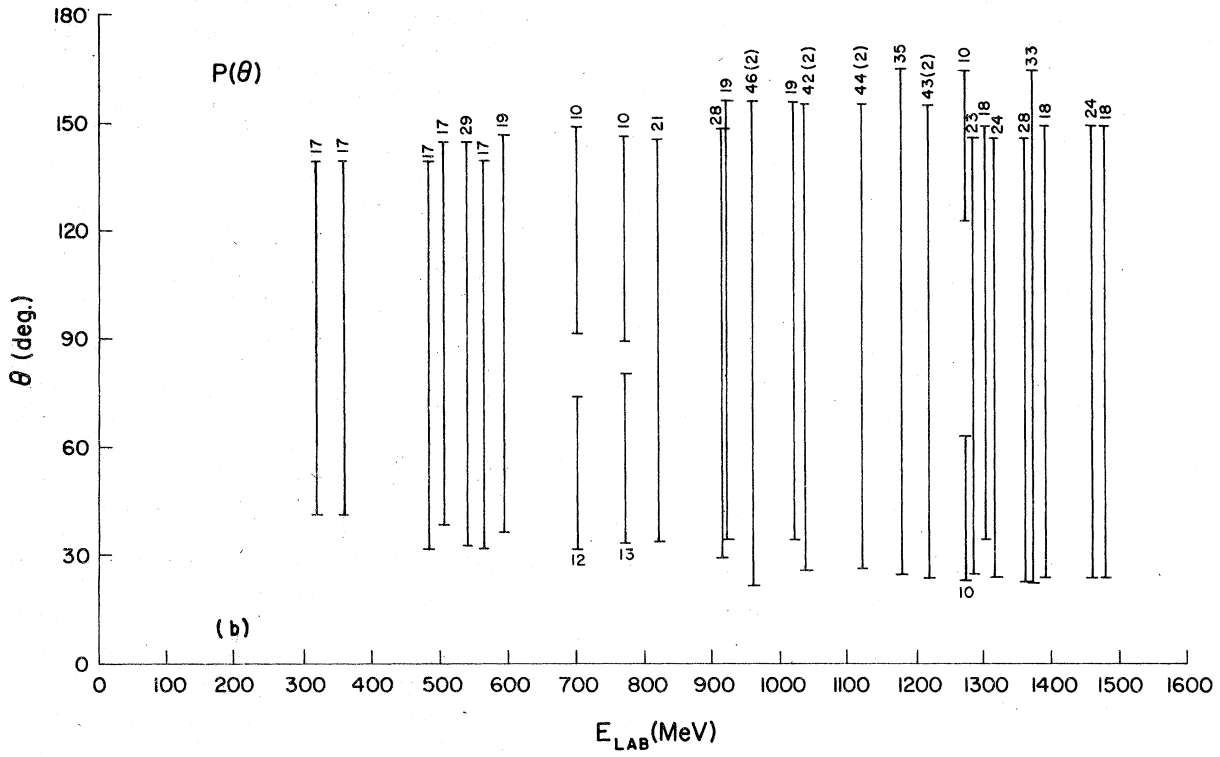

FIG. 1. (*Continued*)

set, even though many of them are quite old and some are inconsistent with each other. (More reaction cross-section measurements would be very helpful to future analyses.) We also kept all polarization values, even though there are large disagreements among them. Details about these disagreements will be given below where the fit results are presented.

All of the data used in the fit are summarized in a more complete report that can be obtained from the second author (L. D. R.). Figure 1 shows the energies and angular ranges of our selected data set.

III. PARAMETRIZATION

The partial-wave parametrization is a coupled-channel K matrix one in which the inelastic effects are represented by one inelastic channel: for the S_{11} state the inelastic channel is the K^*p channel and for the other states the inelastic channel is the $K\Delta$ channel. These specific channels are chosen because they have the lowest orbital angular-momentum state or lowest threshold that communicates with the elastic K^+p channel. The orbital angular momenta l_i for the inelastic channels are given in Table I. The resonances (K^* and Δ) in the inelastic channels are realistically given a Gaussian-smeared mass in the phase-space factors for the channels.

Specifically, the parametrization is as follows: The T matrix is

$$T = \rho^{1/2} K \rho^{1/2} (1 - i\rho^{1/2} K \rho^{1/2})^{-1}, \tag{1}$$

where

TABLE I. Lowest orbital angular momenta of the inelastic channels.

$l_{T,2J}$	S_{11}	P_{11}	P_{13}	D_{13}	D_{15}	F_{15}	F_{17}	G_{17}	G_{19}	H_{19}	$H_{1,11}$
l_i	0	1	1	0	2	1	3	2	4	3	5
	K_*p	$K\Delta$	$K\Delta$	$K\Delta$	$K\Delta$	$K\Delta$	$K\Delta$	$K\Delta$	$K\Delta$	$K\Delta$	$K\Delta$

TABLE II. Width and mass values.

Channel				
K^*N	$\tau_K{}^* = 50$ MeV	$m_K{}^* = 890$ MeV	$m_p = 938.26$ MeV	$m_K = 494$ MeV
$K\Delta$	$\tau_\Delta = 120$ MeV	$m_\Delta = 1240$ MeV	$m_K = 494$ MeV	$m_p = 938.26$ MeV

$$K = \begin{pmatrix} K_e & K_0 \\ K_0 & K_i \end{pmatrix}$$

(for S_{11}, $i \equiv K^*p$; for other states, $i \equiv K\Delta$),

$$\rho = \begin{pmatrix} \rho_e & 0 \\ 0 & \rho_i \end{pmatrix},$$

$\rho_e = Ck^{2l+1}$ where we approximate k at low energies by $k \cong [s - m_k + m_p)]^{1/2}$, s is the square of the c.m. total energy, l is the orbital angular momentum of the elastic channel,

$$\rho_i = \frac{1}{\sqrt{\pi}\tau_\mu} \int_{m_\gamma + m_\pi}^{\infty} [k_i(m_s, m)]^{2l_i+1} \times \exp[-(m - m_\mu)^2/\tau_\mu{}^2]dm ,$$

$k_i(m_s, m) \simeq [s - (m + m_s)^2]^{1/2}$, l_i is the lowest orbital angular momentum of the inelastic channels coupling to l (see Table I). Table II lists the values of the width and mass symbols, and the K-matrix elements are parametrized by

$$K_e = \sum_{n=0}^{N_e} a_n E^n, \quad K_0 = \sum_{n=0}^{N_0} b_n E^n, \quad \text{and } K_i = \sum_{n=0}^{N_i} c_n E^n .$$

The parameters a_n, b_n, and c_n are the parameters which are varied to fit the data. The number of these parameters that are used (N_e, N_0, and N_i) are determined by doing the fit: one wants the minimum number without unduly restricting the freedom of the fit. Generally, the number of parameters decreases about linearly with increasing l because of the short-range nature of the K^+p interaction.

Note that we use powers of the laboratory kinetic energy E rather than laboratory momentum. This is done because E is more simply (linearly) related to s, the square of the c.m. total energy, which is the energy variable that is of greatest theoretical interest, i.e., $E = [s - (m_K + m_p)^2]/2m_p$. We continue to use the old-fashioned E in our data designations rather than the new-fashioned laboratory momentum because of this reason.

IV. SOLUTIONS

The solution we reported previously[1] was one of several that were found that differed only at the high-energy end of the data set. One solution reported here was obtained by starting from zero-parameter values in a 0–100-MeV fit, then increasing the energy range by 100-MeV steps up to 1000 MeV, then fitting our parametrization to the 0–1000-MeV solution and the previous solution above 1000 MeV, and finally varying the parameters for the best fit to the entire 0–1600-MeV data set. After this solution was obtained, energy-band analyses were done in bands of 100-MeV width starting from the 0–1600-MeV solution. It was noticed that the higher-energy bands tended to give a higher S wave than did the 0–1600 solution. Our parametrization was then fitted to the energy-bands' solutions and, by varying the parameters, we found the other solution reported here. The two solutions are similar at low energies. Undoubtedly there are other solutions that differ from these two at the high-energy end, but we feel that the differences between the two reported here indicate the kind of data that are needed to resolve the ambiguities at the high-energy end.

Both of the solutions obtained as described above contain large renormalization of differential cross sections and polarizations at the high-energy end and in the 400–700-MeV range. In an attempt to eliminate this large renormalization we ran both solutions down without any renormalization [solutions H (high S wave) and L (low S wave)]. Then, renormalization was allowed, which yielded solutions (solutions H_r and L_r below) that, as before, contained large renormalization at the high-energy end and in the 400–700-MeV range. (Representation values of the renormalization can be found in Figs. 8–10.)

Figure 2 shows why the renormalization occurs. Consider the high-energy end first: The one σ_r data point at 1373 MeV is obviously inconsistent with the large number of σ_T data points and the σ_{el} values determined by the integration of the $\sigma(\theta)$ data in that energy region. The single σ_r point is not well fitted until renormalization is allowed. In the 400–700-MeV energy region, again, the σ_r, σ_T,

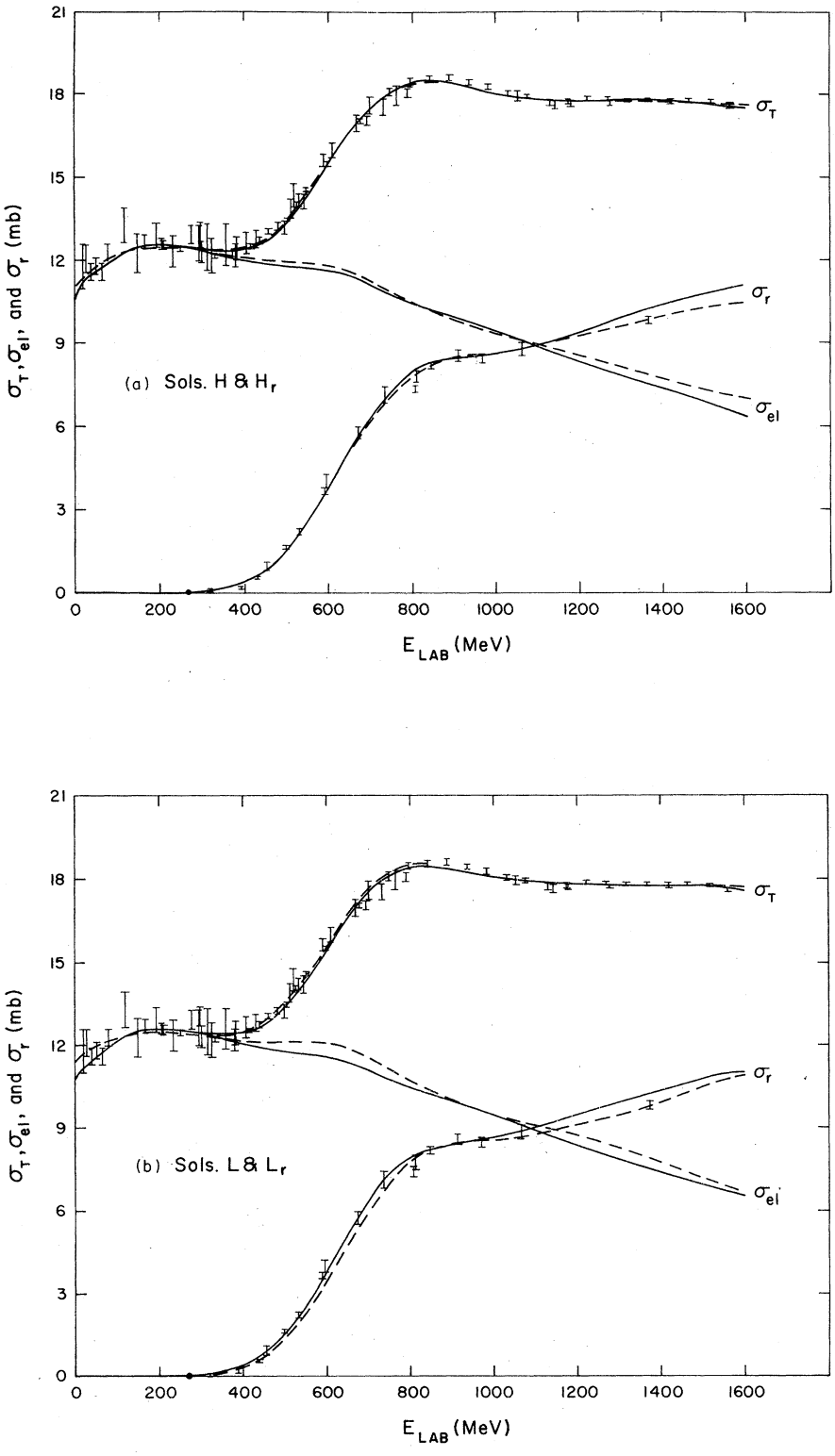

FIG. 2. Our solutions' predictions versus the σ_T and σ_r data. Also shown is the solutions' predictions for σ_{el}. The solid curves are the solutions for which no renormalization was allowed and the dashed curves are the solutions for which renormalization was allowed. (a) Solutions H and H_r. (b) Solutions L and L_r.

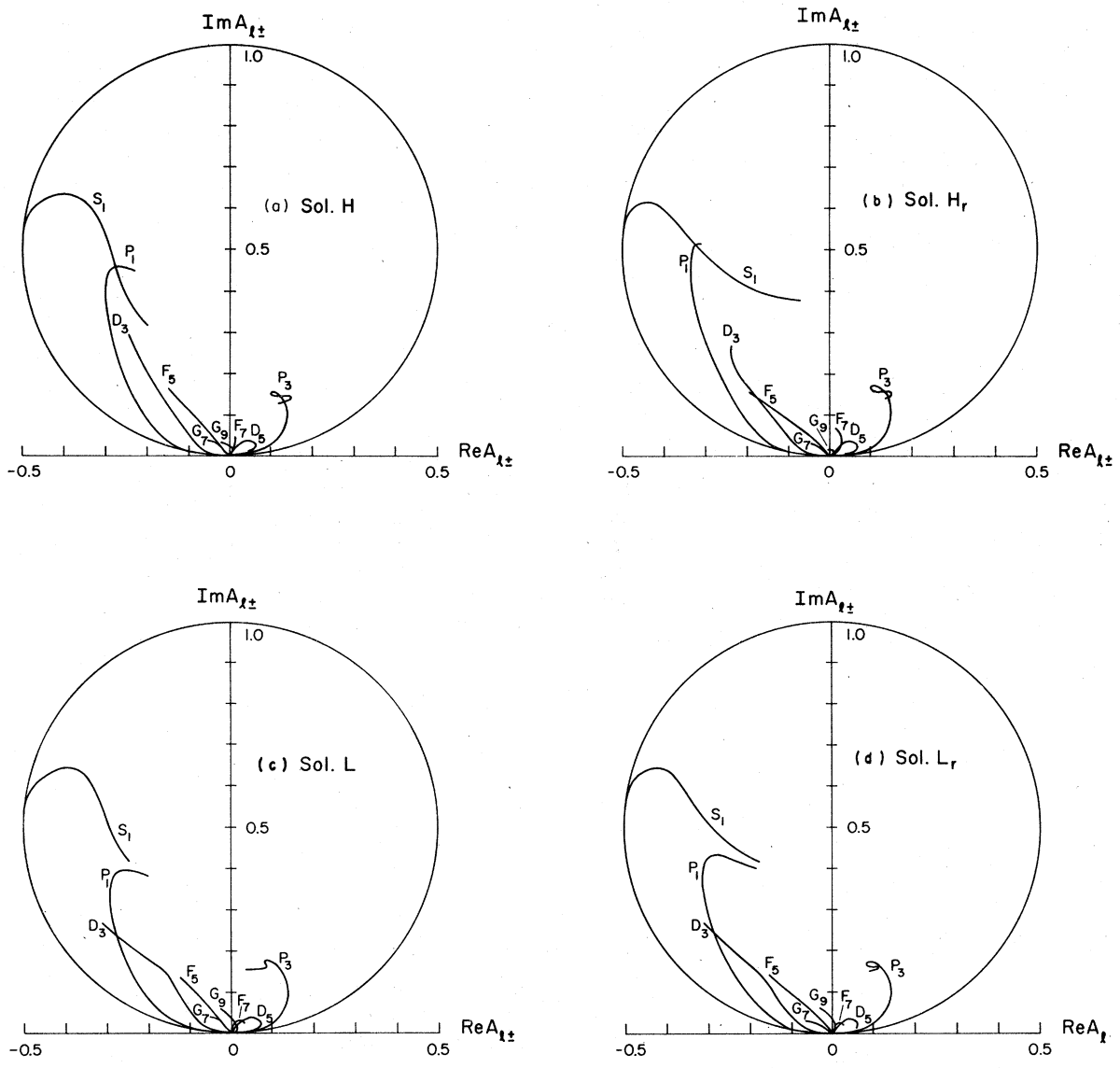

FIG. 3. Argand diagrams for our solutions. (a) Solution H. (b) Solution H_r. (c) Solution L. (d) Solution L_r.

and σ_{el} values are not consistent. The unrenormalized solutions (solutions H and L) fall considerably below the most precise σ_T data but are in reasonable agreement with the σ_r data; whereas the renormalized solutions (solutions H_r and L_r) fall below (particularly L_r) the σ_r data but are in reasonable agreement with the σ_T data. The σ_r data in the 400–700-MeV range were measured between 1962 and 1970, whereas the σ_T data in that range were measured between 1968 and 1973. It appears that some contemporary measurements of σ_r are needed over the entire 0–1600-MeV range.

The Argand diagrams for all four solutions, excluding H waves, are shown in Fig. 3, and the phase shifts and absorption parameters of all four solutions are shown in Figs. 4 and 5. Tables of all of the fit parameters and partial-wave amplitudes for the solutions are available from the second author (L. D. R).

There are 3006 data in our data set. Table III lists the χ^2 values and χ^2/(data point) for the four solutions mentioned above.

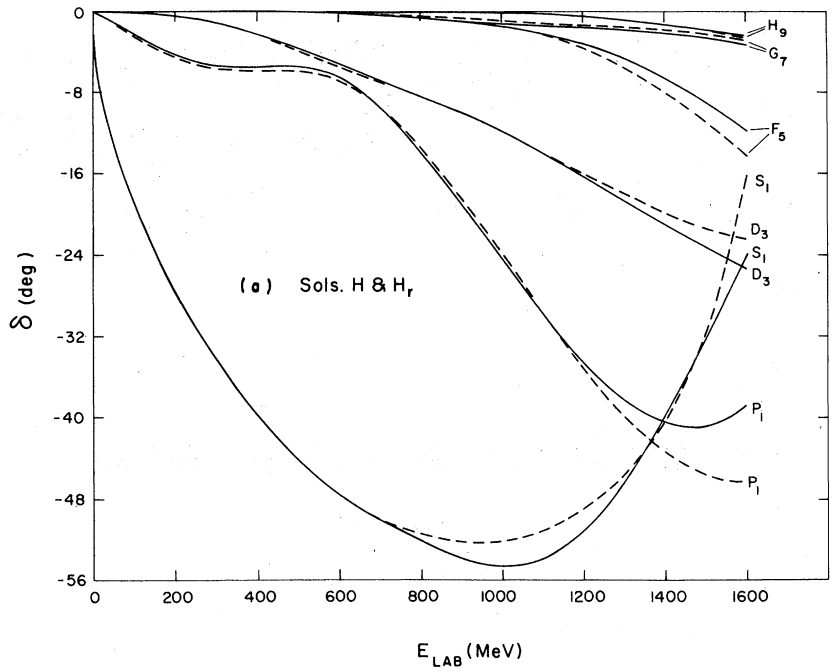

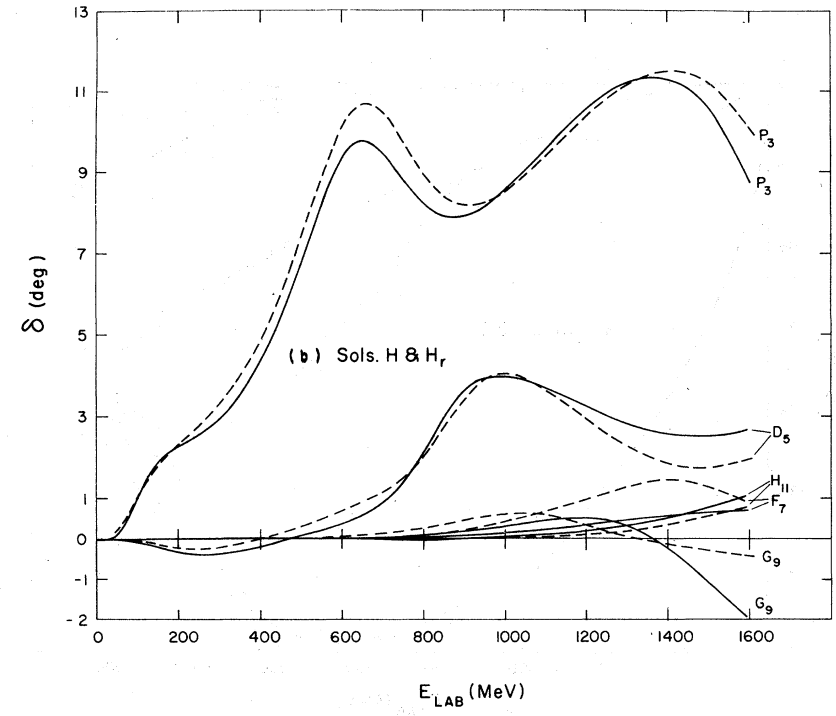

FIG. 4. Phase shifts and absorption parameters for our H and H_r solutions. The solid curves are solutions in which no renormalization was allowed (H) and the dashed curves are the solutions in which renormalization was allowed (H_r). (a) Phase shifts for $l=0$ and $j=l-\frac{1}{2}$ partial waves. (b) Phase shifts for $j=l+\frac{1}{2}$ partial waves. (c) Absorption parameters for all partial waves.

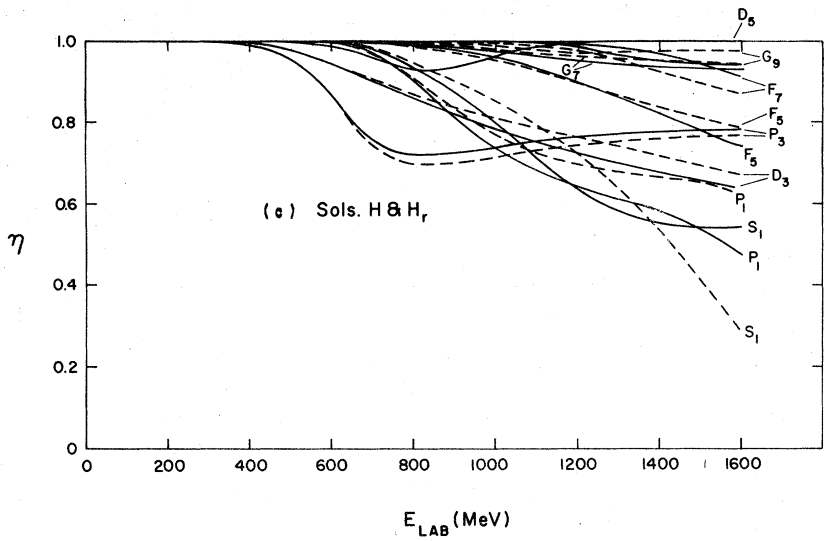

FIG. 4. (*Continued*)

We shall later discuss some of the characteristics of these solutions after observing how well the data are fitted by the solutions. We discuss mainly the unrenormalized solutions (solutions H and L) in this paper because of the extreme amount of renormalization that exists in the renormalized solutions.

Unfortunately, the data inconsistencies are so

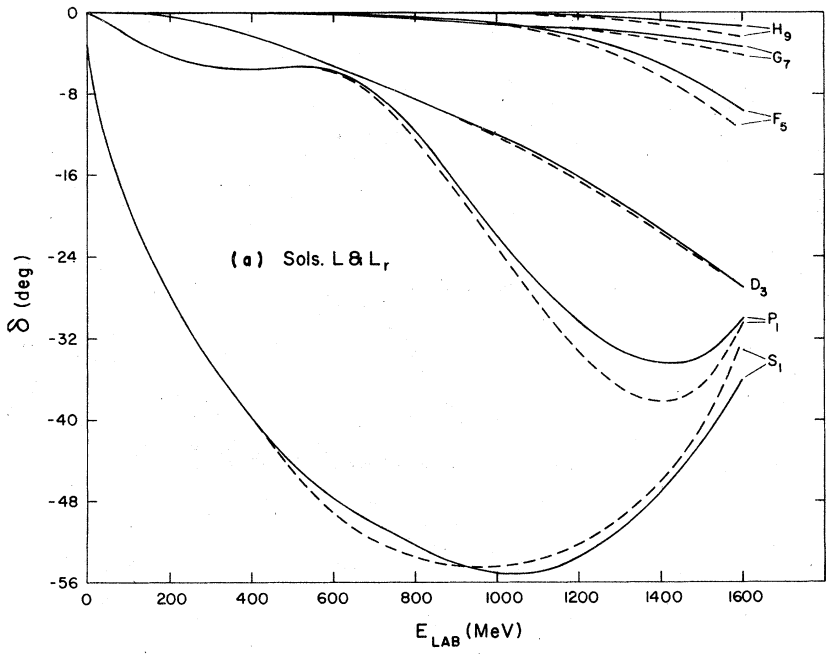

FIG. 5. Phase shifts and absorption parameters for our L and L_r solutions. The solid curves are solutions in which no renormalization was allowed (L) and the dashed curves are the solutions in which renormalization was allowed (L_r). (a) Phase shifts for $l=0$ and $j=l-\frac{1}{2}$ partial waves. (b) Phase shifts for $j=l+\frac{1}{2}$ partial waves. (c) Absorption parameters for all partial waves.

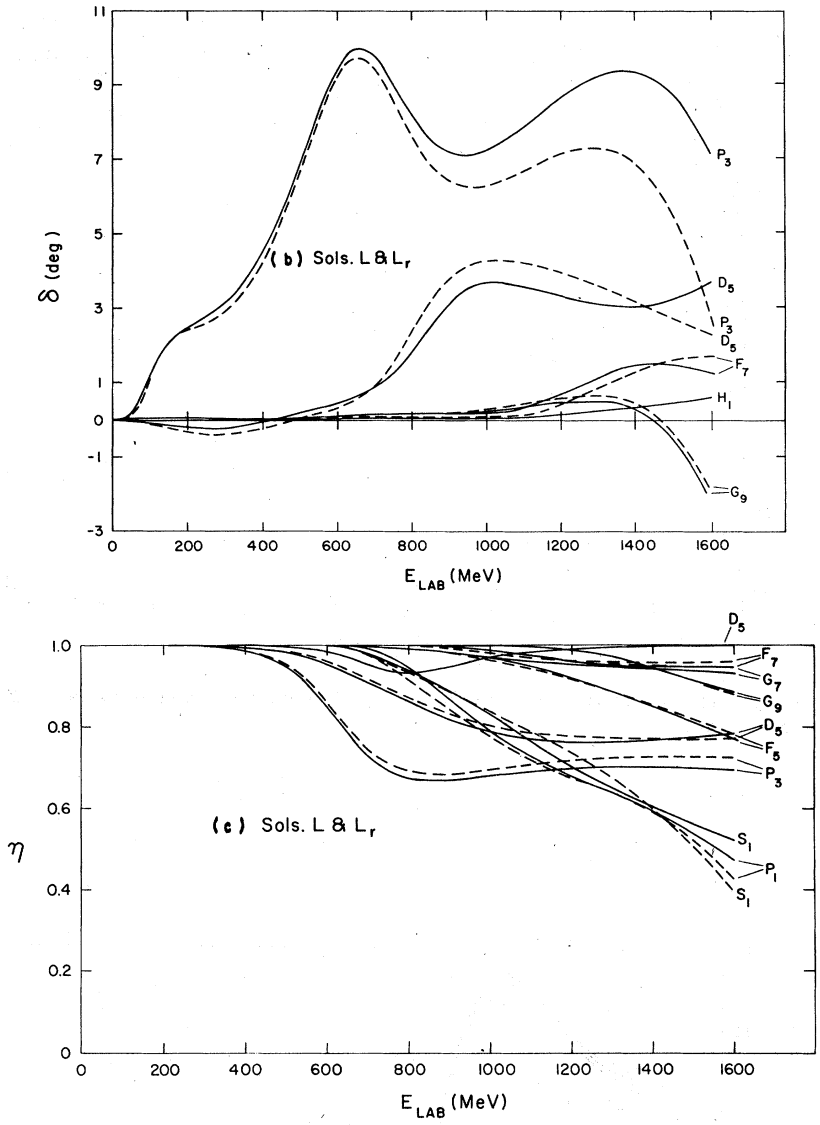

FIG. 5. (*Continued*)

bad, even after elimination of many data, that we were not able to obtain an error matrix for our solutions. The differences among our solutions can be taken as a measure of the solutions' uncertainties.

V. FITS TO THE DATA

First, consider the fit to the $\alpha = \mathrm{Re}f(0)/\mathrm{Im}f(0)$ "data" as shown in Fig. 6. All four solutions yield essentially the same curve; all are considerably

TABLE III. χ^2 and χ^2 (data point) for the H, H_r, L, and L_r solutions.

Solution	H	H_r	L	L_r
χ^2	5194	3745	5174	3774
χ^2/(data point)	1.73	1.25	1.72	1.26

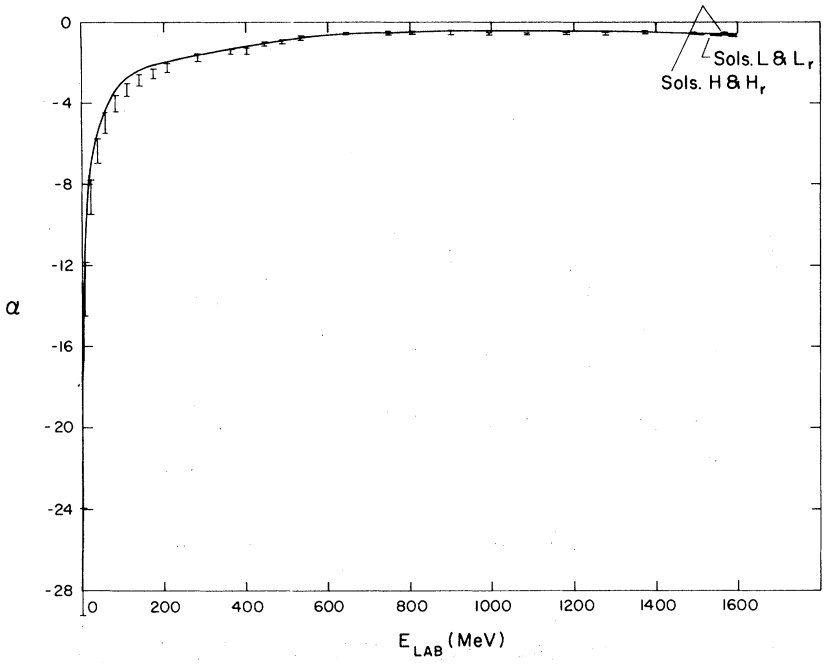

FIG. 6. Our solutions' predictions versus the $\alpha = \mathrm{Ref}(0)/1\,mf(0)$ "data". The solid curve is the H or H_r solution; the dashed curve is the L or L_r solution.

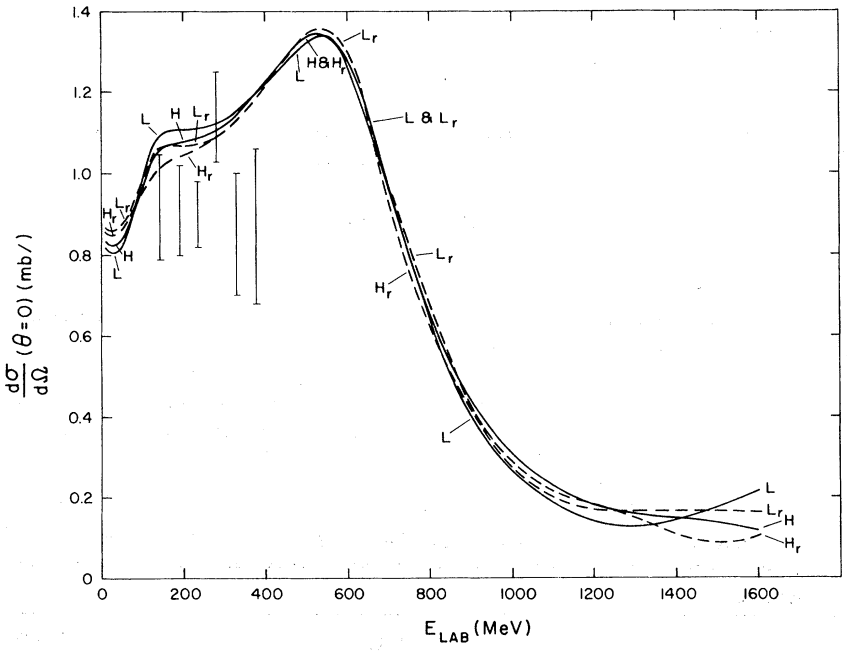

FIG. 7. Our solutions' predictions versus the $\sigma(0)$ data. The solid curves are the H and L solutions; the dashed curves are the H_r and L_r solutions.

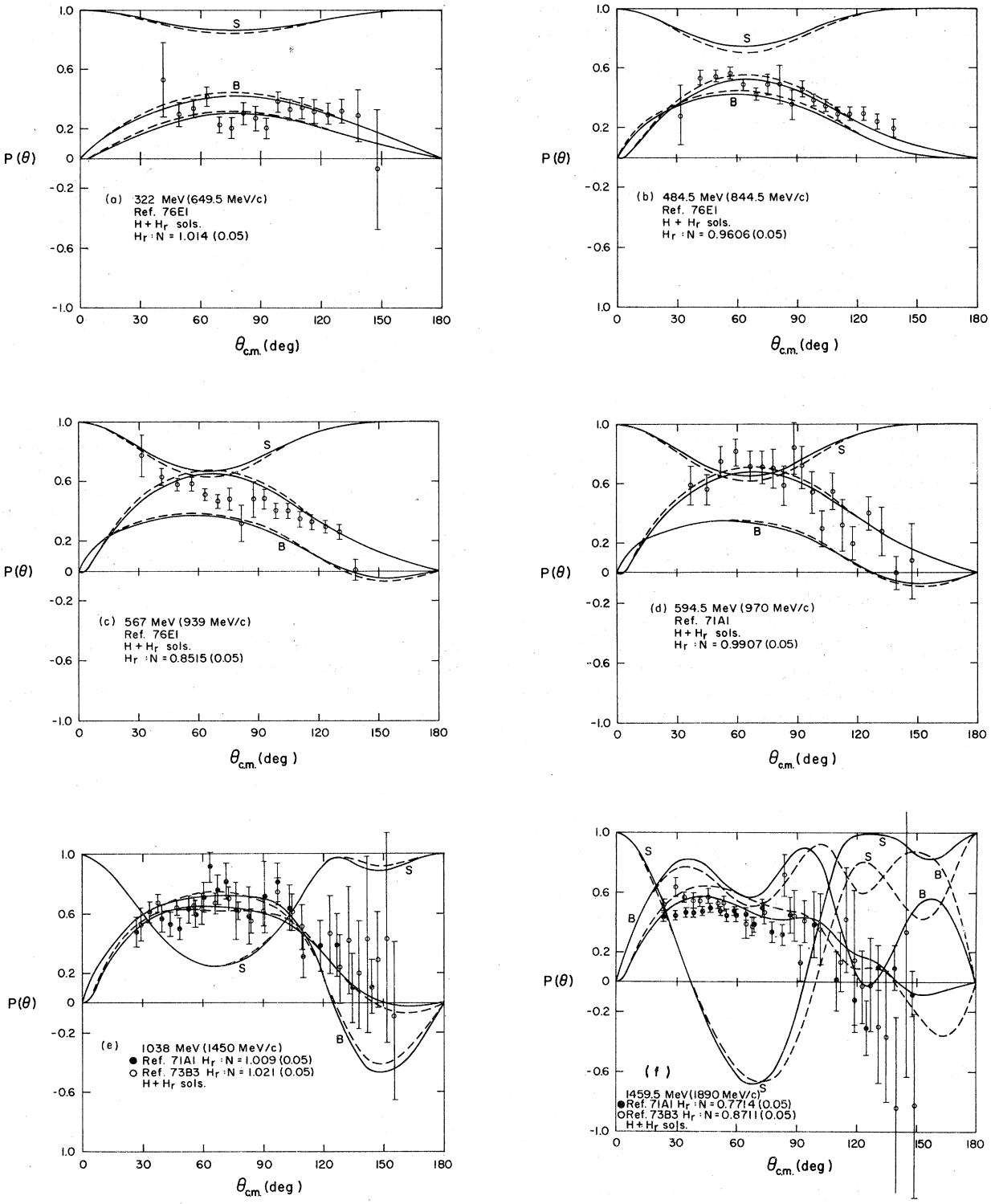

FIG. 8. Our H and H_r solutions' predictions versus the polarization data at selected energies. The solid curve is the H solution and the dashed curve is the H_r solution. Also, curves for the H and H solutions' predictions for $S(\theta)$ and $B(\theta)$ are labeled by S and B. The renormalization factors N are given: the data are to be divided by this factor. The normalization error is given in parentheses. (a) 322 MeV. (b) 484.5 MeV. (c) 567 MeV. (d) 594.5 MeV. (e) 1038 MeV. (f) 1459.5 MeV.

above the data values. We could not find any solution that would yield a curve as low as the data.

There are six data for $\sigma(0)$, whose agreement with the four solutions is shown in Fig. 7. Five of the data are considerably below and one is in good agreement with the curves. All data are from the same reference (70C2).

The most important data are, of course, the polarization data. Fits of the H and H_τ solutions to some of the polarization data are shown in Fig. 8. Also shown are predictions for

$$B(\theta) \equiv \frac{-2\,\mathrm{Re}[f^*(\theta)g(\theta)]}{|f(\theta)|^2 + |g(\theta)|^2}$$

and

$$S(\theta) \equiv \frac{|f(\theta)|^2 - |g(\theta)|^2}{|f(\theta)|^2 + |g(\theta)|^2},$$

where $f(\theta)$ is the non-spin-flip amplitude and $g(\theta)$ is the spin-flip amplitude. The L and L_τ solutions differ from the H and H_τ solutions in the fits to the polarization data only near the high end of the energy range. Figure 9 shows the L and L_τ fits to the polarization at the highest energy shown in Fig. 8. Note that the low-energy data of data reference 76E1 [Figs. 8(a)–8(c)] are low in the intermediate angle region as compared to our solutions and the nearby data of data reference 71A1 [Fig. 8(d)].

Finally, we present in Fig. 10 the H and H_τ solutions' fits to a small set of the differential cross-section data. The L and L_τ solutions' fits are not sufficiently different than the H and H_τ solutions' fits to warrant showing them.

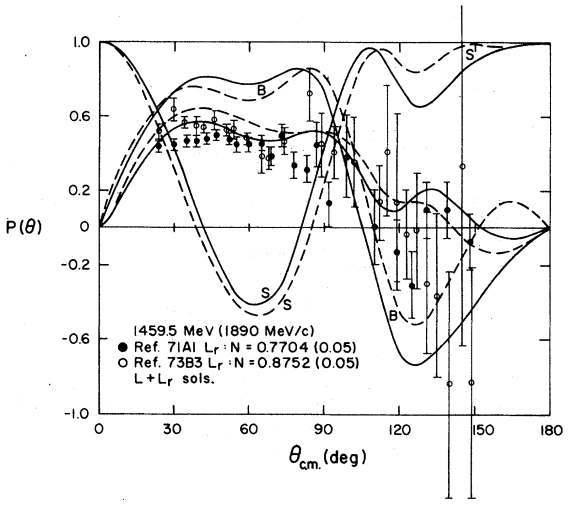

FIG. 9. Our L and L_τ solutions' predictions versus the polarization data at 1459.5 MeV. The solid curve is the L solution and the dashed curve is the L_τ solution. Also, curves for the L and L_τ solutions' predictions for $S(\theta)$ and $B(\theta)$ are labeled by S and B. The renormalization factors N are given: the data are to be divided by this factor. The normalization error is given in parentheses.

To give a birds-eye view of our H and L solutions' predictions for $P(\theta)$, $S(\theta)$, and $B(\theta)$, we

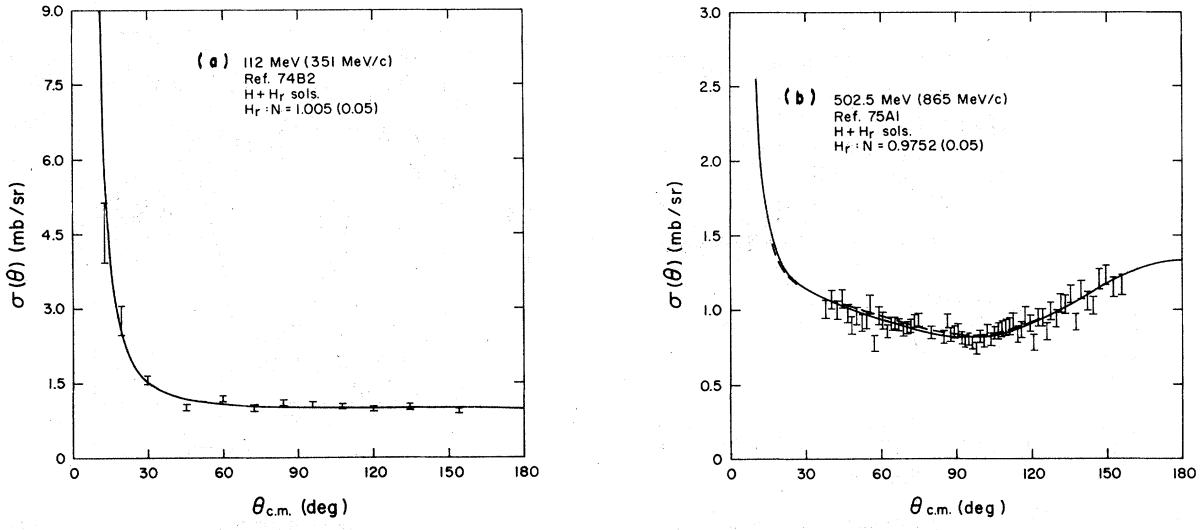

FIG. 10. Our H and H_τ solutions' predictions versus the differential-cross-section data at selected energies. The solid curve is the H solution and the dashed curve is the H_τ solution. The renormalization error factors N are given: the data are to be divided by this factor. The normalization error is given in parentheses. (a) 112 MeV. (b) 502.5 MeV. (c) 906 MeV. (d) 1532.5 MeV.

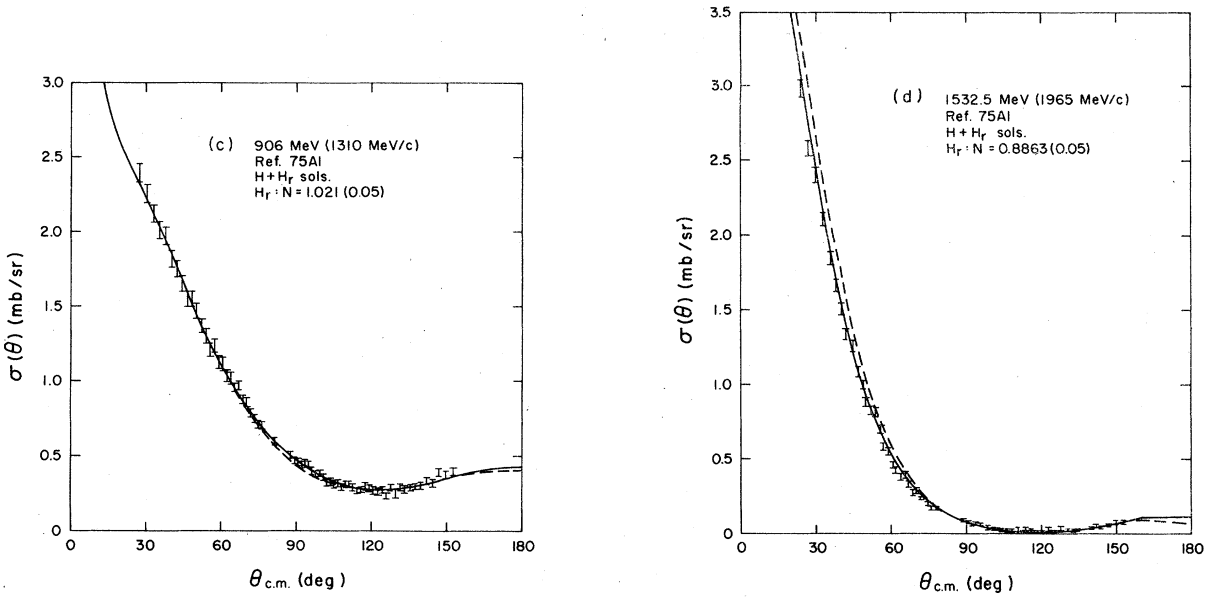

FIG. 10. (*Continued*)

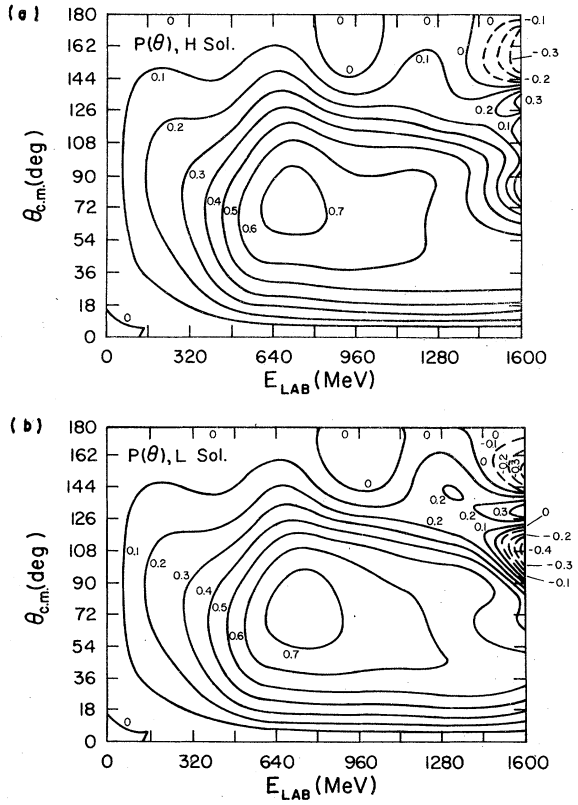

FIG. 11. Contour plots for polarization predictions of our H and L solutions. The lines of constant $P(\theta)$ are labeled. Positive values of $P(\theta)$ are solid lines and negative values are dashed lines.

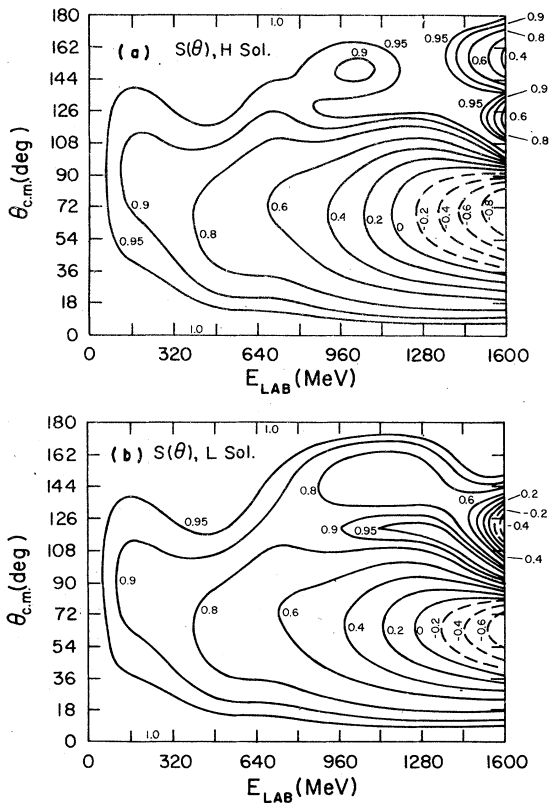

FIG. 12. Contour plots for $S(\theta)$ predictions of our H and L solutions. The lines of constant $S(\theta)$ are labeled. Positive values of $S(\theta)$ are solid lines and negative values are dashed lines.

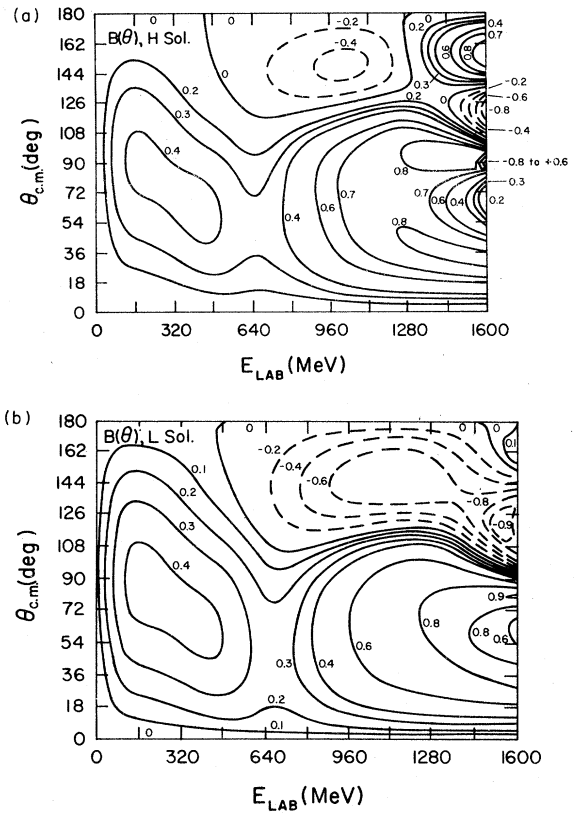

FIG. 13. Contour plots for $B(\theta)$ predictions of our H and L solutions. The lines of constant $B(\theta)$ are labeled. Positive values of $B(\theta)$ are solid lines and negative values are dashed lines.

present contour plots of them in Figs. 11–13. We believe that this way of presenting predictions should be very useful to experimentalists who are planning future experiments. We shall discuss below the future experiments that we believe are most needed.

VI. CHARACTERISTICS OF THE SOLUTIONS

One can see in Figs. 4 and 5 that the four solutions agree reasonably well below 1000 MeV. We believe that the character of the solution is well determined below 1000 MeV. The P_{13} resonance reported in Ref. 1 manifests itself in the data at about 800 MeV, so we believe that the P_{13} resonance is well established. Our four solutions differ very little in the location of the P_{13} resonance pole in the complex total c.m. energy plane, as shown in Table IV.

Besides the P_{13} resonances, seasoned resonance hunters will recognize in Figs. 3–5 the hints of resonances in other partial waves. A search for resonance-type poles in the complex total c.m energy plane yields the results shown in Table IV. In perusing Table IV the reader should bear in mind that the threshold for K^+p scattering is 1432 MeV total c.m. energy and the end of our analysis' energy range (1567 MeV laboratory kinetic energy) is 2234 MeV total c.m. energy. Of course, the pole position given in Table IV does not directly indicate where the main effect of the resonance will be on the real energy axis—that depends on the energy dependence of the Breit-Wigner resonance widths (elastic and inelastic) and of the background. In fact, these energy dependences can be so violent that a nearby resonance pole is not visually obvious in the partial wave. The only way to assure that a resonance pole exists is to find the pole in the complex total c.m. energy plane in every solution that fits the scattering data. All of the poles in Table II, except the P_{13} pole, are far from the real axis (>200 MeV) or are near the end of our analysis' energy range (e.g., G_{19}). We conclude that the P_{13} resonance pole is well established and that there are strong hints for resonance poles in other states which must await confirmation by means of more precise and reliable polar-

TABLE IV. Resonance-pole positions for our solutions. Note that all but the P_3 and G_9 are very weak because they are far from the real axis. The G_9 is weak because it is highly inelastic (see Figs. 4 and 5). Therefore, all but the P_3 should be taken as hints of possible resonances. We also find a hint of a S_1 resonance near ($-115i$ MeV) the real axis about 300 MeV above the end point (2234 MeV) of our analysis range.

State	Solutions L	L_r	H	H_r
P_1	1703–324i	1725–335i	1719–328i	1722–333i
P_3	1795–106i	1797–107i	1796–101i	1798–105i
D_5	1761–215i	1779–235i	1778–229i	1800–238i
F_5	2046–380i	2004–346i	2016–353i	1954–298i
F_7	1863–387i	1851–362i	2427–309i	2192–206i
G_7	1680–310i	1680–310i	1680–310i	1680–310i
G_9	2201–162i	2205–163i	2127–140i	2022–111i

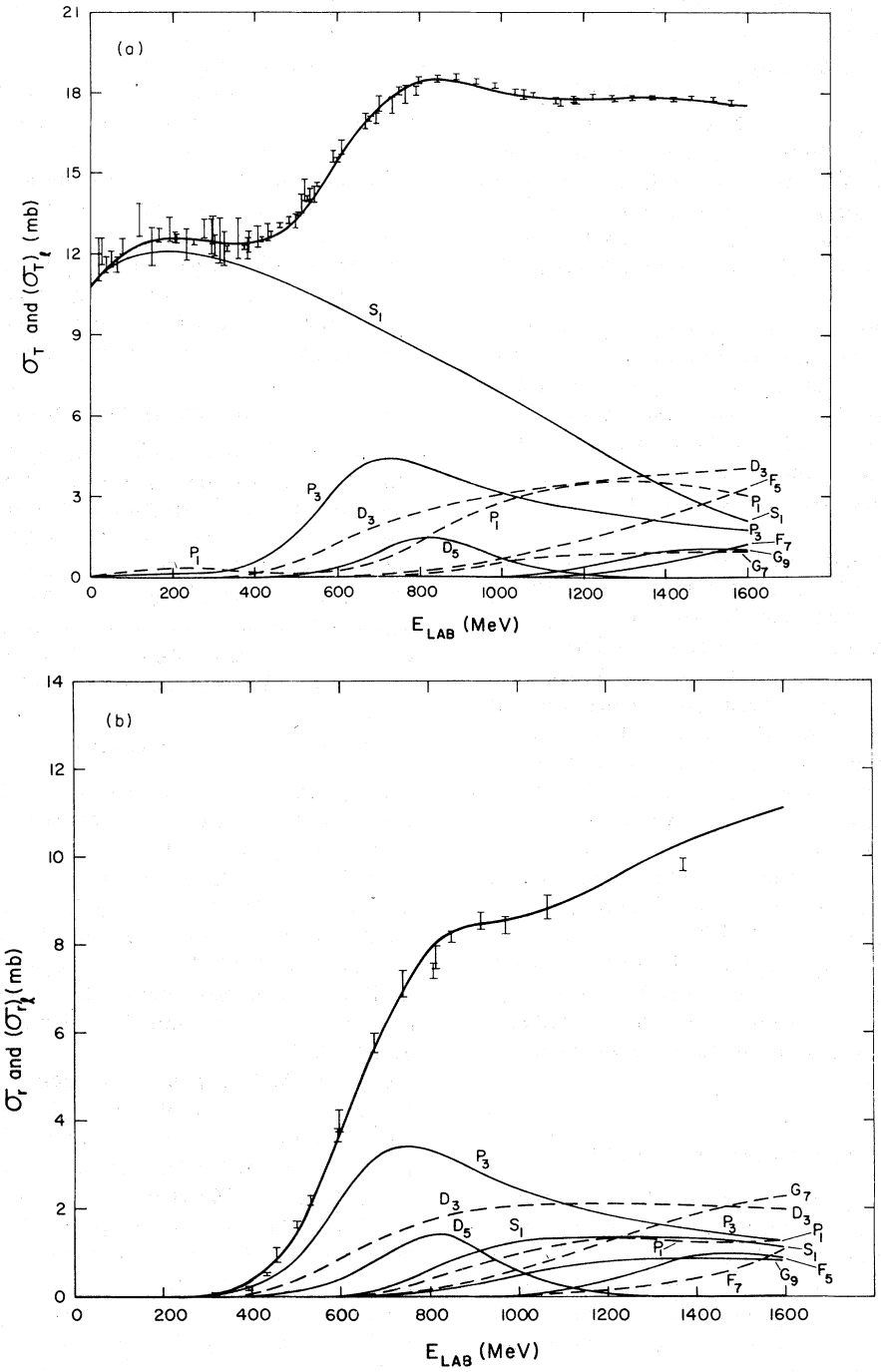

FIG. 14. Partial-wave contributions to the total and reaction cross sections for solid H. The heavy solid curve is the sum of all partial waves; the light solid curves are the $j = l + \frac{1}{2}$ partial waves, and the dashed curves are the $j = l - \frac{1}{2}$ partial waves. (a) Total cross section. (b) Reaction cross section.

ization measurements. We know of no solution that fits the current data set that does not have a P_{13} resonance pole.

The P_{13} resonance pole position real part varies only by three MeV for our four solutions, but the imaginary part varies by six MeV. We recommend the H solution pole position $(1796 - 101i)$ as a canonical value for the P_{13} pole until further data become

available to further refine the analysis.

The D_{15} argand plots in Fig. 3 have an unusual behavior—they curl sharply in a clockwise direction and apparently will curl sharply back counterclockwise at energies above our cutoff energy. Our parametrization actually has a resonant pole at 1761 to 1800 MeV on the real axis and 215 to 238 on the imaginary axis. We hope to soon extend our analysis to higher energies to see if this D_{15} and the other resonance pole positions in Table III remain.

Figure 14 shows how the various partial wave contribute to the total and reaction cross sections. Note that, although the resonant P_{13} is dominant in the sudden rise in the 500–800-MeV energy range, the D_{13} and D_{15} also make important contributions to the rise. Also, note that the $j = l - \frac{1}{2}$ partial waves initially rise faster than do the $j = l + \frac{1}{2}$ partial waves.

Note in Figs. 4 and 5 that the $j = l - \frac{1}{2}$ phase shifts are all negative and, except for the s wave, the $j = l + \frac{1}{2}$ phase shifts are usually positive.

Another interesting behavior in our solutions is the P_{13} phase-shift behavior below 300 MeV as shown in Fig. 4(b). This behavior is caused by the recent polarization measurements of data reference 76E1. As mentioned in the previous section, these data have some unusual features. Therefore, we suggest that other measurements of low-energy polarizations are needed.

Figures 3, 4, and 5 lead one to believe in the possibility of a reasonably elastic S_{11} resonance above our energy range (>2 GeV/c). Indeed, we find an S_{11} resonance pole in all of our solutions at about $2500 - i115$ MeV. We are presently collecting data up to 3 GeV/c in order to extend our analysis to higher energies and see if the S_{11} does have a strong resonance.

VII. SUGGESTED FUTURE EXPERIMENTS

There is a great need for more reliable experimental data in order to better determine the partial-wave amplitudes in K^+p scattering.

(a) Reaction cross sections. Our analysis indicates that there are inconsistencies among the measured total cross sections, reaction cross sections, and the elastic cross sections determined by the integration of the $\sigma(\theta)$ data. Since the reaction-cross-section data are the oldest data and since the reaction-cross-section data are crucial to the determination of the absorption parameters, we urge that new efforts be made to measure K^+p reaction cross sections at intervals of 50 MeV between 500 and 1600 MeV.

(b) Polarization. Figure 8 shows that there are large discrepancies among the available polarization data. For example, compare Fig. 8(c) and Fig. 8(d), the data in Fig. 8(e), and the data in Fig. 8(f). There is a great need for refinements in polarization-measurement techniques that will lead to reliable and precise values for the polarization. The authors will, with pleasure, aid any experimentalists in determining the most desireable energies and angles at which polarization measurements should be made.

(c) Spin rotation parameters (S and B). It appears from Fig. 8 that, in our energy range, measurements of $S(\theta)$ and $B(\theta)$ would be of most use at the highest energies and highest angles (>90°).

VIII. ACKNOWLEDGMENTS

The authors wish to thank Barry Lovett for providing the data of data reference 76E1 prior to publication, Dr G. E. McClellan for providing the reaction datum of data reference 77M1 prior to publication, and Dr. R. Patton for providing tables of the data of reference 75P1. Dr. Roger Hackman was involved in the early stages of this work. This work as made possible by grants from the Energy Research and Development Administration.

APPENDIX

The data used in our fit are from the following references. All except the starred references are as numbered in Ref. 8.

62F1 J. Fisk, K. Ticho, D. H. Stork, W. Chinowsky, G. Goldhaber, S. Goldhaber, and T. F. Stubbs, CERN Conference 358, 1962 (unpublished).

65B1 A. Bettini, M. Cresti, S. Limentani, L. Peruzzo, R. Santangelo, D. Locke, D. J. Crennel, W. T. Davies, and P. B. Jones, Phys. Lett. 6, 83 (1965).

67F1 T. A. Filippas, V. P. Henri, B. Jongejans, M. Krammer, J. M. Perreau, S. Focardi, A. Minguzzi-Ranzi, L. Monari, G. Saltini, P. Serra, E. Barrelet, E. Huffer, and F. Muller, Nuovo Cimento A51, 1053 (1967).

67F2 S. Focardi, A. Minguzzi-Ranzi, L. Monari, G. Saltini, P. Serra, T. A. Filippas, and V. P. Henri, Phys. Lett. B24, 314 (1967).

68B1 D. V. Bugg, R. S. Gilmore, K. M. Knight, D. C. Salter, G. H. Stafford, E. J. N. Wilson, J. D. Davies, J. D. Dowell, P. M. Hattersley, R. J. Homer, A. W. O. Dell, A. A. Carter, R. J. Tapper, and K. F. Riley, Phys. Rev. 168, 1467 (1968).

69B2 R. W. Bland, M. G. Bowler, J. L. Brown, J. A. Kadyk, G. Goldhaber, S. Goldhaber, V. H. Seeger, and G. H. Trilling, Nucl. Phys. 138, 595 (1969).

70A1 R. J. Abrams, R. L. Cool, G. Giacomelli, T. F. Kycia, A. B. A. Leontic, K. K. Li, and D. N.

Michael, Phys. Rev. D 1, 1917 (1970).

70B1 T. Bowen, P. K. Caldwell, F. N. Dikmen, E. W. Jenkins, R. M. Kalbach, D. V. Petersen, and A. E. Pifer, Phys. Rev. D 2, 2599 (1970).

70C1 R. L. Cool, G. Giacomelli, T. K. Kycia, B. A. Leontic, K. K. Li, A. Lundby, J. Teiger, and C. Wilkin, Phys. Rev. D 1, 1887 (1970).

70C2 P. K. Caldwell, T. Bowen, F. N. Dikmen, E. W. Jenkins, R. M. Kalbach, D. F. Petersen, and A. E. Pifer, Phys. Rev. D 2, 1 (1970).

70G1 G. Giacomelli, P. Lugaresi-Serra, G. Mandrioli, A. M. Rossi, F. Griffiths, I. S. Hughes, D. A. Jacobs, R. Jennings, B. C. Wilson, G. Ciapetti, V. Costantini, G. Martellotti, D. Zanello, E. Castelli, and M. Sessa, Nucl. Phys. B20, 301 (1970).

71A1 M. G. Albrow, S. Andersson-Almehed, B. Bosnjakovic, C. Daum, F. C. Erne, Y. Kimura, J. P. Lagnaux, J. C. Sens, F. Udo, and F. Wagner, Nucl. Phys. B30, 273 (1971).

71E1 R. D. Ehrlich, A. Etkin, P. Glodis, V. W. Hughes, K. Kondo, D. C. Lu, S. Mori, R. Patton, G. A. Rebka, Jr., J. E. Rothberg, P. A. Thompson, and M. E. Zeller, Phys. Rev. Lett. 26, 1925 (1971).

72C1 B. J. Charles, I. M. Cowan, T. R. M. Edwards, W. M. Gibson, A. R. Gillman, R. G. Gilmore, M. H. Gledhill, C. M. Hughes, J. Malos, V. J. Smith, R. J. Tapper, B. McCartney, D. L. Ward, P. D. Wroath, G. A. Beck, M. Coupland, and S. G. F. Frank, Ruth. Lab. Report No. PP/H/95, 1972 (unpublished).

72L1 S. C. Loken, B. C. Barish, R. Gomez, D. W. Davies, P. E. Schlein, and W. Slater, Phys. Rev. D 6, 2346 (1972).

73A1 C. J. Adams, G. F. Cox, J. D. Davies, J. D. Dowell, T. Dimbylow, G. H. Grayer, M. Hattersley, R. J. Homer, R. J. Howells, C. McLeod, T. J. McMahon, H. B. van der Raay, L. Rob, C. J. S. Damerell, and M. J. Hotchkiss, Nucl. Phys. B66, 36 (1973).

73B1 T. Bowen, E. W. Jenkins, R. M. Kalbach, D. V. Petersen, A. E. Pifer, and P. K. Caldwell, Phys. Rev. D 7, 22 (1973).

73B3 B. A. Barnett, A. T. Laasanen, P. F. M. Koehler, P. H. Steinberg, J. G. Asbury, J. D. Dowell, D. Hill, H. Kato, D. Lundquist, T. B. Novey, A. Yokosawa, G. Burleson, D. Eartly, and K. Pretzl, Phys. Rev. D 8, 2751 1973).

73B4 A. Berthon, L. Montanet, E. Paul, P. Saetre, D. M. Sendall, P. Bertranet, G. Burgun, E. Lesquoy, A. Muller, E. Pauli, and S. Zylberajch, Nucl. Phys. B63, 54 (1973).

73C1 A. S. Carroll, T. F. Kycia, K. K. Li, D. N. Michael, P. M. Mockett, D. C. Rahm, and R. Rubinstein, Phys. Lett. B45, 531 (1973).

74B1* R. A. Burnstein, J. J. LeFebvre, D. V. Petersen, H. A. Rubin, T. B. Day, J. R. Fram, R. G. Glasser, G. McClellan, B. Zechi-Zorn, and G. A. Snow, Phys. Rev. D 10, 2767 (1974).

74C1 W. Cameron, A. A. Hirata, R. Jennings, W. T. Norton, E. Cazzoli, G. Giacomelli, P. Lugaresi-Serra, G. Mandrioli, A. Minguzzi-Ranzi, E. Castelli, P. Poropat, C. Omero, and M. Sessa, Nucl. Phys. B78, 93 (1974).

75A1* K. Abe, B. A. Barnett, J. H. Goldman, A. T. Laasanen, P. H. Steinbert, G. J. Marmer, D. R. Moffett, and E. F. Parker, Phys. Rev. D 11, 1719 (1975).

75P1* R. Patton, W. A. Barletta, R. D. Ehrlich, A. Etkin, P. A. Souder, M. E. Zeller, M. Mishina, and D. M. Lazarus, Phys. Rev. Lett. 34, 975 (1975) and private communication from R. Patton.

76B1* P. Baillon, C. Bricman, M. Ferro-Luzzi, P. Jenni, J. M. Perreau, R. D. Tripp, and T. Ypsilantis, Nucl. Phys. B105, 365 (1976).

76B2* P. Baillon, Y. Déclais, M. Ferro-Luzzi, P. Jenni, J. M. Perreau, J. Séguinot, and T. Ypsilantis, Nucl. Phys. B107, 189 (1976).

77E1* R. D. Ehrlich, B. Lovett, M. Mishina, I. Nakano, J. Snyder, P. A. Souder, M. E. Zeller, and D. M. Lazarus, private communication (1977).

77M1* G. E. McClellan and B. Zorn, private communication (1977).

---

[1]R. A. Arndt, R. H. Hackman, L. D. Roper, and P. H. Steinberg, Phys. Rev. Lett. 33, 987 (1974).

[2]B. R. Martin, in *Proceedings of the Topical Conference on Baryon Resonances, Oxford, 1976*, edited by R. T. Ross and D. H. Saxon (Rutherford Laboratory, Chilton, Didcot, England, 1977).

[3]R. D. Ehrlich, B. Lovett, M. Mishina, I. Nakano, J. Snyder, P. A. Souder, M. E. Zeller, and D. M. Lararus, Yale-Brookhaven Report, 1975 (unpublished), and private communication from B. Lovett, 1977.

[4]B. R. Martin, Nucl. Phys. B94, 413 (1975).

[5]K. Abe, B. A. Barnett, J. H. Goldman, A. T. Laasanen, P. H. Steinberg, G. J. Marmer, D. R. Moffett, and E. F. Parker, Phys. Rev. D 11, 1719 (1975).

[6]R. Patton, W. A. Barletta, R. D. Ehrlich, A. Etkin, P. A. Souder, M. E. Zeller, M. Mishina, and D. M. Lazarus, Phys. Rev. Lett. 34, 975 (1975) and private communication from R. Patton (1976).

[7]R. E. Cutkosky, H. R. Hicks, J. Sandusky, C. C. Shih, R. L. Kelly, R. C. Miller, and A. Yokosawa, Nucl. Phys. B102, 139 (1976).

[8]U. Casadei, G. Giacomelli, P. Lugaresi-Serra, G. Mandrioli, A. M. Rossi, and F. Viaggi, CERN Report No. CERN/HERA 75-1, 1975 (unpublished).